CrO_4 distortion-driven ferroelectric order in $(R,Y)CrO_4$ (R = Sm, Gd, and Ho): A new family of multiferroics

A. Indra,[1,2] K. Dey,[1,3] J. K. Dey,[1] S. Majumdar,[1] U. Rütt,[4] O. Gutowski,[4] M. v. Zimmermann,[4] and S. Giri[1,*]

[1]*Department of Solid State Physics, Indian Association for the Cultivation of Science, Jadavpur, Kolkata 700032, India*

[2]*Department of Physics, Srikrishna College, Bagula, Nadia, W. B. 741502, India*

[3]*Department of Physics, SBSS Mahavidyalaya, Goaltore, Paschim Medinipur, W. B. 721128, India*

[4]*Deutsches Elektronen-Synchrotron DESY, Notkestr. 85, 22603 Hamburg, Germany*

(Received 28 March 2018; revised manuscript received 22 May 2018; published 5 July 2018)

We report a new multiferroic family of $(R,Y)CrO_4$ (R = Sm, Gd, and Ho). The ferroelectric ordering temperatures are observed at much higher temperatures than their corresponding magnetic ordering temperatures for all the members. The values of electric polarization (P) are significantly high, which vary from ~217 to ~640 $\mu C/m^2$ for a 4 kV/cm poling field. The large value of P (~590 $\mu C/m^2$) for $YCrO_4$ compared to the smallest P value in the series for $GdCrO_4$ signifies that the magnetic rare-earth element does not directly influence the P value. Our careful analysis of the low-temperature synchrotron diffraction studies confirms that the distortion of CrO_4 tetrahedra directs the P value. The structural transformation from the centrosymmetric $I4_1/amd$ structure to a noncentrosymmetric $I\bar{4}2d$ space group at the onset of polar order is found to be correlated with the appearance of spontaneous electric polarization.

DOI: 10.1103/PhysRevB.98.014408

I. INTRODUCTION

The compounds with the RXO_4-type chemical formula are interesting for the fundamental structural issues [1,2] and promising for the geophysical and geochronological applications [3,4]. The compounds with R = rare earth and X = P, As, Cr, and V typically adopt the zircon or monazite-type structure at an ambient condition and change to the scheelite-type polymorph at the high pressures and moderate temperatures [5–8]. In addition to the structural instabilities, these series of compounds attract the community for their intriguing magnetic [9–11] and optical properties [12–14]. Over the last few decades, interesting magnetic properties have been realized for RVO_4 [15–21] and $RCrO_4$ [22–25].

The $RCrO_4$ family of our interest attracts special attention for the unusual outer shell electronic configuration ($3d^14s^0$) of Cr^{5+} ions and the peculiar superexchange paths offered by the zircon-type structure. Here, the superexchange paths between R^{3+} ions are mediated either by the direct linkage of polyhedra (R^{3+}–O^{2-}–R^{3+}) or through the CrO_4 tetrahedra (R^{3+}–O^{2-}–Cr^{5+}– O^{2-}–R^{3+}), as depicted in Fig. 1. Figure 1 further depicts the formation of edge-sharing zigzag chains composed of RO_8 bisdisphenoid polyhedra along a axis. The chains of RO_8 bisdisphenoid polyhedra are connected through the edges of CrO_4 tetrahedra along c axis. Thus direct linkage between R^{3+} – O^{2-} – R^{3+} follows the shorter superexchange path. The contrast magnetic order has been proposed in $RCrO_4$ series. The antiferromagnetic (AFM) order has been reported for R = Nd, Sm, Eu, Yb, Lu [23–26] whereas ferromagnetic (FM) order was settled for R = Gd, Er, Tm [22,27,28,35] with the zircon-type structure having tetragonal $I4_1/amd$ space group. The above results were authenticated by the neutron depolarization and diffraction studies [27–34]. Recently, an unusual metamagnetism driven by coexisting FM and AFM interactions was proposed in $DyCrO_4$ [2,35]. Few members of $RCrO_4$ with R = Gd, Dy, and Ho have been recognized as promising candidates for magnetic refrigeration at low temperatures, where a crucial role of the $3d$-$4f$ hybridization was proposed for accounting for the observed extraordinary large magnetocaloric effect [36–38]. Significant structural instability has been observed in $RCrO_4$ where it adopted either the zircon-type structure having $I4_1/amd$ space group or the tetragonal scheelite-type structure with $I4_1/a$ space group depending on the sample synthesis conditions. Importantly, the magnetism is strongly influenced by the structural instability. For example, $HoCrO_4$ and $TbCrO_4$ were found FM with the zircon-type structure and AFM for the scheelite-type structure [39,40]. Analogous to that observed in $RCrO_4$, the FM superexchange was observed with a Curie temperature of about 9 K for the zircon phase whereas the AFM superexchange was realized for the scheelite phase with a Néel temperature of 21 K for $YCrO_4$ [6,8].

Experimental evidence using the photoelectron spectroscopy indicated that $YCrO_4$ was a robust insulator [41]. The *ab initio* calculations proposed that the tetrahedral coordination of the Cr^{5+} ions led a crucial role for providing a large band gap in $YCrO_4$ as well as $RCrO_4$ series [1,2,41–43]. As a consequence of highly insulating conductivity, these candidates are expected to be suitable for ferroelectric order in cases when the space inversion symmetry breaks. Our meticulous studies confirm the emergence of a polar order ranging from 98 to 108 K for few members of $RCrO_4$ (R = Sm, Gd, and Ho) series as well as $YCrO_4$, which crystallize in the zircon-type structure at room temperature. Reasonably high values of electric polarization are observed in the range

*Corresponding author: sspsg2@iacs.res.in

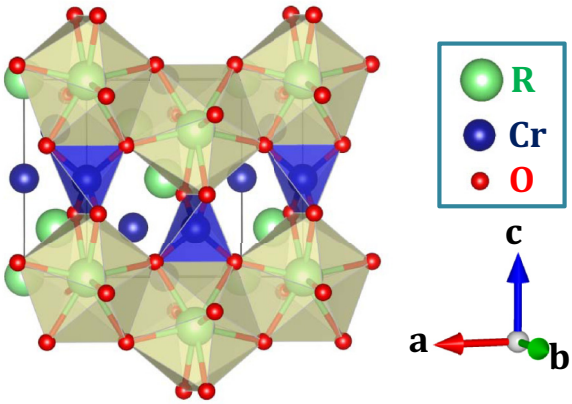

FIG. 1. Direct linkage of polyhedra (RO_8) along a axis or linkage through the CrO_4 tetrahedra along c axis.

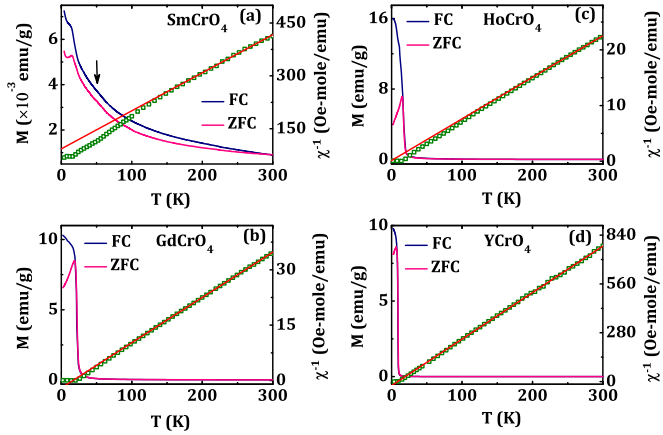

FIG. 2. Temperature dependence of FC-ZFC magnetization curves for (a) $SmCrO_4$, (b) $GdCrO_4$, (c) $HoCrO_4$, and (d) $YCrO_4$ at 100 Oe. Arrow in (a) indicates a weak anomaly around 50 K. The right axes show the corresponding inverse of the magnetic susceptibility [χ^{-1}(T)] and the Curie-Weiss fit (solid line).

from ~217 to ~640 μC/m^2 for a 4 kV/cm poling field. The structural transformation from the centrosymmetric $I4_1/amd$ structure to a noncentrosymmetric $I\bar{4}2d$ structure at the onset of polar order is found to be correlated with the appearance of spontaneous electric polarization. The large polarization value of ~590 μC/m^2 is striking for $YCrO_4$ and confirms that the magnetic rare-earth cation does not influence significantly the occurrence as well as the value of spontaneous electric polarization. All low-temperature synchrotron diffraction studies of $SmCrO_4$ and $YCrO_4$ propose that the distortion of CrO_4 octahedra is rather crucial for the occurrence of polar order and magnitude of spontaneous electric polarization. The results reveal a new family of isomorphous (R,Y)CrO_4 belonging to the elite members of multiferroics.

II. EXPERIMENTAL DETAILS

The polycrystalline $RCrO_4$ (R = Sm, Gd, and Ho) and $YCrO_4$ are prepared using a solid-state reaction [24]. The single phase chemical composition is confirmed by the x-ray diffraction studies at room temperature recorded in a Bruker D8 Advance powder diffractometer using the Cu K_α radiation. The single-phase chemical composition is further checked by the synchrotron x-ray diffraction studies recorded with a wavelength of 0.1259 Å(98 keV) at the P07 beamline of PETRA III, Hamburg, Germany in the temperature range of 10–300 K. The synchrotron powder diffraction data are analyzed using the Rietveld refinement with the commercially available MAUD and FULLPROF softwares. The powder sample pressed into a pellet is used for the dielectric measurements using a E4980A LCR meter (Agilent Technologies, USA) equipped with a commercial PPMS evercool-II system of Quantum Design. The pyroelectric current (I_p) is recorded in an electrometer (Keithley, model 6517B) at a constant temperature sweep rate. The I_p is integrated over time for obtaining the spontaneous electric polarization (P). The poling electric fields are applied during cooling processes and all the measurements are carried out in the warming mode in zero electric field. Before measurement of I_p, the electrical connections are short circuited and left idle for a sufficiently long time. In all measurements, the electrical contacts are fabricated using an air drying silver paint. The temperature dependence of heat capacity (C_p) is measured in a PPMS of Quantum Design. Magnetization is measured in a commercial magnetometer of Quantum Design (MPMS, evercool).

III. EXPERIMENTAL RESULTS AND DISCUSSIONS

Thermal variations of the zero-field cooled (ZFC) and field-cooled (FC) magnetization curves recorded at 100 Oe are displayed in Figs. 2(a), 2(b), 2(c), and 2(d) for $SmCrO_4$, $GdCrO_4$, $HoCrO_4$, and $YCrO_4$, respectively. In accordance with the reported AFM ordering, a peak is observed at ~15 K (T_N) for $SmCrO_4$ [23–25]. As indicated by the arrow in Fig. 2(a) a weak anomaly is noted in both the ZFC and FC magnetization curves, which may occur due to a short-range ordering. This weak signature is also noted in the structural parameters as discussed later. The ZFC magnetization curve deviates from the FC curve below ~280 K, which is much above T_N. This indicates a dominant short-range magnetic order above T_N for $SmCrO_4$. In contrast, as reported for $GdCrO_4$ [22,28,32,36,38], $HoCrO_4$ [37,38,40], and $YCrO_4$ [6,33], the FM orders are noted at ~22, ~18, and ~9 K, respectively. The magnetic hysteresis loops are recorded below the transition temperatures as depicted in Figs. 3(a), 3(b), 3(c), and 3(d) for $SmCrO_4$, $GdCrO_4$, $HoCrO_4$, and $YCrO_4$, respectively. A nearly linear magnetization curve at 4 K is consistent with the proposed AFM order. An exactly linear curve is observed at 40 K for $SmCrO_4$. The magnetization curves for $GdCrO_4$, $HoCrO_4$, and $YCrO_4$ exhibit the FM-like nonlinear behavior below FM T_C. The low coercivities propose a soft ferromagnetic character of the compounds. For $HoCrO_4$, the curve at 4 K shows a saturating trend at 50 kOe, whereas it shows a complete saturation of magnetization for $GdCrO_4$ and $YCrO_4$ at 4 and 2 K, respectively.

The inverse of the magnetic susceptibilities (χ^{-1}) with T are depicted in Figs. 2(a), 2(b), 2(c), and 2(d) for $SmCrO_4$, $GdCrO_4$, $HoCrO_4$, and $YCrO_4$, respectively. In all cases, the χ^{-1}(T) deviates from the linearity at a temperature much higher their magnetic ordering temperatures. From the high-temperature linear Curie-Weiss fit, the effective paramagnetic

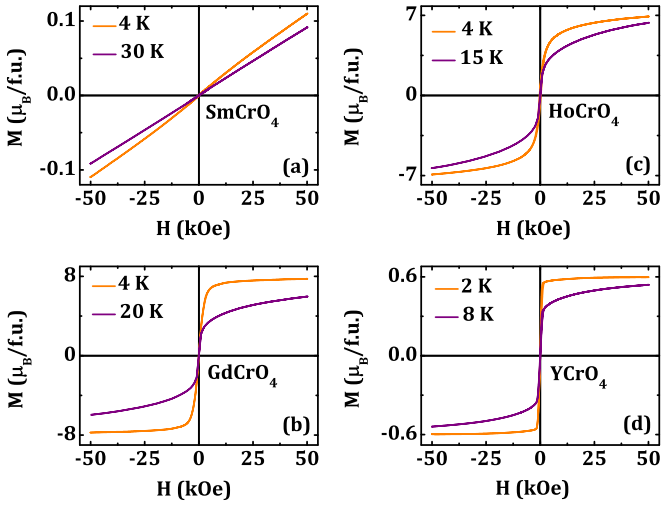

FIG. 3. Magnetization curves at selective temperatures for (a) $SmCrO_4$, (b) $GdCrO_4$, (c) $HoCrO_4$, and (d) $YCrO_4$.

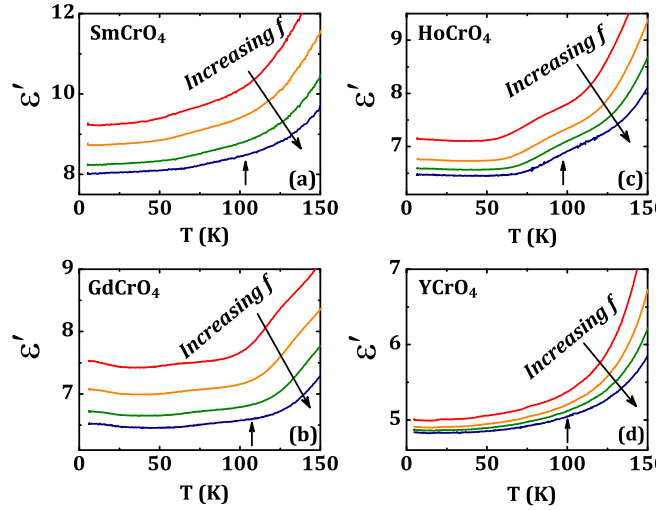

FIG. 4. The T variations of real component of dielectric permittivities (ϵ') at different frequencies (f) for (a) $SmCrO_4$, (b) $GdCrO_4$, (c) $HoCrO_4$, and (d) $YCrO_4$.

moment (μ_{eff}) and Curie-Weiss temperature (Θ_{CW}) are listed in Table I for all the compounds. The values of μ_{eff} are quite close to the corresponding theoretical values (μ_{theo}). The values of saturation moment (M_S) below the FM T_C are quite close to the corresponding μ_{eff} values for $GdCrO_4$, $HoCrO_4$, and $YCrO_4$. The value of magnetization at 50 kOe for $SmCrO_4$ is much smaller than the values for $GdCrO_4$ and $HoCrO_4$, which occurs due to low moment of Sm^{3+}. The negative Θ_{CW} indicates strong AFM interactions for $SmCrO_4$. For the rest of the compounds, the small values of Θ_{CW} associated with a large μ_{eff} suggest the existence of both AFM and FM interactions of comparable strength.

The dielectric permittivities (ϵ) are recorded at different frequencies (f) by varying T for all four compounds. Figures 4(a), 4(b), 4(c), and 4(d) depict thermal variation of the real components (ϵ') of ϵ at f = 2, 5, 10, and 20 kHz for $SmCrO_4$, $GdCrO_4$, $HoCrO_4$, and $YCrO_4$, respectively. The $\epsilon'(T)$ plots demonstrate a weak anomaly or a change of slope in the $\epsilon'(T)$ curve, as indicated by the arrows in the figure. The weak signature may be attributed to the overlapping of the intrinsic component with the extrinsic components in ϵ such as the grain boundary and the sample-electrode interface effects. Here, the arrows indicate the onset of the spontaneous electric polarization. The details of which are discussed further later. We further note that this anomaly is not clearly observed for $YCrO_4$. In order to solve this issue, we have incorporated specific heat capacity measurements for $YCrO_4$. Figure 5 shows the $C_P(T)$ of $YCrO_4$. A peak in the low-T region corresponds to the magnetic ordering temperature, as indicated by the arrow. In addition, a weak anomaly or a change of slope is also observed around ~100 K (inset of the figure), at which temperature the onset of the polar order is noted for $YCrO_4$.

The magnetodielectric (MD) or magnetocapacitance effects are investigated at low temperature for all the reported members of $RCrO_4$ series. The MD effects, defined as $\epsilon'(H)/\epsilon'(0) - 1$, are depicted with H in Figs. 6(a)–6(d) for $SmCrO_4$, $GdCrO_4$, $HoCrO_4$, and $YCrO_4$, respectively. Here, the $\epsilon'(H)$ and $\epsilon'(0)$ represent the ϵ' with H and $H = 0$, respectively. The H variation of MD effect is similar for $GdCrO_4$ and $HoCrO_4$. The value of $\epsilon'(H)/\epsilon'(0) - 1$ increases with H up to ~0.4 and 0.65 % at 50 kOe for Gd and Ho compounds, respectively. For the Y compound, the $[\epsilon'(H)/\epsilon'(0) - 1] - H$ plot also behaves similarly up to ~42 kOe, above which the

TABLE I. Magnetic and ferroelectric parameters of $RCrO_4$.

	Magnetic					Ferroelectric	
System	$T_N(T_C)$ K	Θ_{CW} K	μ_{eff} μ_B	μ_{theo} μ_B	M_S μ_B	T_C K	P $\mu C/m^2$
$SmCrO_4$	15	−86	2.38	1.92	-	103	290
$GdCrO_4$	22	+16.5	7.70	8.12	6.9	108	217
$HoCrO_4$	18	+1.5	9.86	10.74	7.8	98	640
$YCrO_4$	9	+9.0	1.64	1.73	0.6	100	590

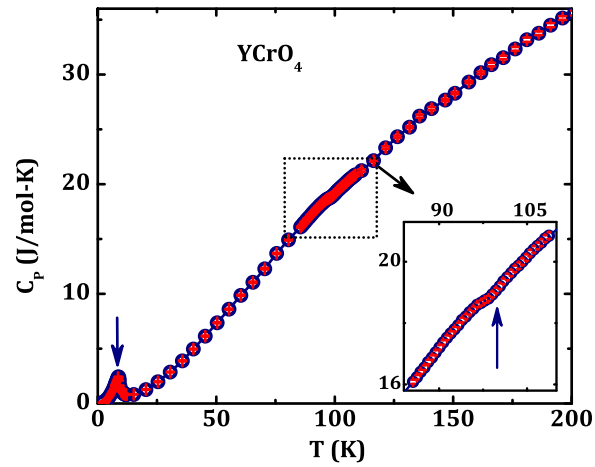

FIG. 5. The T variation of heat capacity (C_p) for $YCrO_4$. The arrow at low temperature indicates FM ordering temperature. The inset shows the highlighted region of C_p. The arrow in the inset depicts the FE ordering temperature.

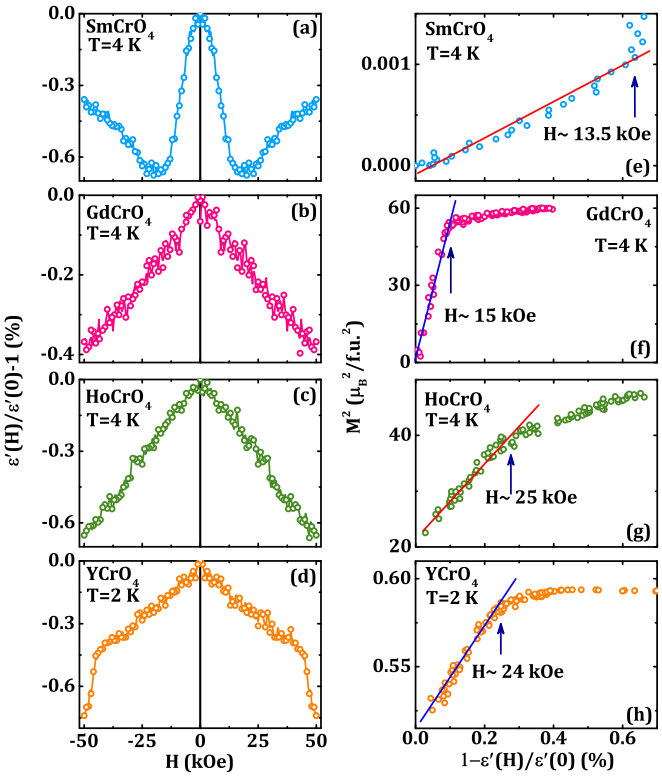

FIG. 6. The H variation of $\epsilon'(H)/\epsilon'(0) - 1$ for (a) $SmCrO_4$, (b) $GdCrO_4$, (c) $HoCrO_4$, and (d) $YCrO_4$. The M^2 vs $-[\epsilon'(H)/\epsilon'(0) - 1]$ plots for (e) $SmCrO_4$, (f) $GdCrO_4$, (g) $HoCrO_4$, and (h) $YCrO_4$.

$\epsilon'(H)/\epsilon'(0) - 1$ decreases sharply to the value of ~0.75 % at 50 kOe for $YCrO_4$. Unlike the rest of the compounds, $\epsilon'(H)/\epsilon'(0) - 1$ initially decreases rapidly up to ~0.65 % around ~20 kOe, above which $\epsilon'(H)/\epsilon'(0) - 1$ increases to ~0.36 % monotonically at 50 kOe for $SmCrO_4$. We note that the values of $\epsilon'(H)/\epsilon'(0) - 1$ are considerable and comparable to the reported results for different multiferroics such as $CoCr_2S_4$ [44], MCr_2O_4 (M = Mn, Co, Ni) [45,46], $BiMnO_3$ [47], $ZnCr_2O_4$ [48], and Sm_2BaNiO_5 [49]. The MD effect relates the ME coupling, which can be phenomenologically expressed using the Ginzburg-Landau theory through the ME coupling term $\gamma P^2 M^2$ in the thermodynamic potential (Φ) defined as

$$\Phi = \Phi_0 + \alpha P^2 + \frac{\beta}{2} P^4 - PE + \alpha' M^2 + \frac{\beta'}{2} M^4 - MH + \gamma P^2 M^2, \quad (1)$$

where α, β, α', β', and γ are the constants and functions of temperature. In the magnetically ordered state, the role of magnetic order on MD in a field is followed by the linear curve of M^2 versus $[\epsilon'(H)/\epsilon'(0) - 1](\%)$ in the low-field region. Here, the M^2 versus $-[\epsilon'(H)/\epsilon'(0) - 1](\%)$ plots at 4 K for $SmCrO_4$, $GdCrO_4$, and $HoCrO_4$, and at 2 K for $YCrO_4$ are depicted in Figs. 6(e)–6(h), respectively. We note that the linearity of the curve holds satisfactorily below ~13.5, 15, 25, and 24 kOe for $SmCrO_4$, $GdCrO_4$, $HoCrO_4$, and $YCrO_4$, respectively. The results indicate that the ME coupling term $\gamma P^2 M^2$ of the Ginzburg-Landau theory [Eq. (1)] is significant for all the reported members of $RCrO_4$ series, as reported earlier for various multiferroics [44–49].

In order to confirm the spontaneous polar order, the pyroelectric currents (I_p) are recorded with T for all the samples in different conditions. A peak in $I_p(T)$ is observed for all the samples, as evident in Figs. 7(a), 7(c), 7(e), and 7(g) for $SmCrO_4$, $GdCrO_4$, $HoCrO_4$, and $YCrO_4$, respectively, which are recorded at different heating rates. The peaks of $I_p(T)$ curves appear at 103, 108, 98, and 100 K for $SmCrO_4$, $GdCrO_4$, $HoCrO_4$, and $YCrO_4$, respectively. The integral of I_p over time for the three curves at different heating rates provide a reproducible value of $P(T)$. Furthermore, the peak temperature does not change at different heating rates. This indicates that the trapped charges involving a thermally stimulated current [50], if exist, do not contribute to the measured pyroelectric currents. The polarization (P) with T for different poling fields (E) is depicted in Figs. 7(b), 7(d), 7(f), and 7(h) for $SmCrO_4$, $GdCrO_4$, $HoCrO_4$, and $YCrO_4$, respectively. The reversal of P due to a change in sign of E (± 4 kV/cm) signifies ferroelectric behavior of the compounds. The E-dependent polarization results are also depicted in the figures by varying E values from −2 to −4 kV/cm. The P values increase with E, pointing to the fact that the P does not saturate for E at 4 kV/cm. The values of P are considerable and vary from ~217 to ~640 μC/m^2 for $E = 4$ kV/cm, as given in Table I. We further note that the ferroelectric (FE) transition (T_C) for all the compounds occurs at much higher temperatures than their respective magnetic transition temperatures, as listed in Table I. Importantly, the values of FE T_C are observed significantly below the temperatures around which the $\chi^{-1}(T)$ deviates from the Curie-Weiss behavior at ~200, ~150, ~225, and ~130 K, for $SmCrO_4$, $GdCrO_4$, $HoCrO_4$, and $YCrO_4$, respectively. The results may indicate that the appearance of the polar order is correlated with the short-range magnetic order for all the compounds, which has been found recently in few occasions [49,51–53]. In the above cases, a structural transition to the noncentrosymmetric structure around FE ordering was established as the origin of the FE order.

In the current observation, the values of P are not systematic with the systematic variation of ionic radii of R^{3+}. In fact, the magnetic R^{3+} or nonmagnetic Y^{3+} does not systematically influence the value of P as well as the FE T_C. In order to address these issues, low-temperature synchrotron diffraction studies over a wide temperature range of 10–300 K are carried out for a magnetic representative at the R site, such as $SmCrO_4$, and a nonmagnetic representative at the R site, for example, $YCrO_4$. Figures 8(a) and 8(d) show the diffraction patterns at two selective temperatures below (90 K) and above (110 K) the FE T_C for $SmCrO_4$ and $YCrO_4$, respectively. The insets of the figures highlight the changes of intensities of (200) and (600) peaks above and below the FE T_C. The changes of the (600) diffraction peak around the FE T_Cs from 110 K to 90 K are depicted with the small temperature intervals in Figs. 8(b) and 8(e). Here, the (600) peak at different temperatures is vertically shifted for the clarification of the changes of peak positions. The small shifts in the peak positions are shown around the FE T_Cs for both the compounds, indicating changes in the lattice constants. Temperature variations of the integrated intensities of the (200) diffraction peaks for $SmCrO_4$ and

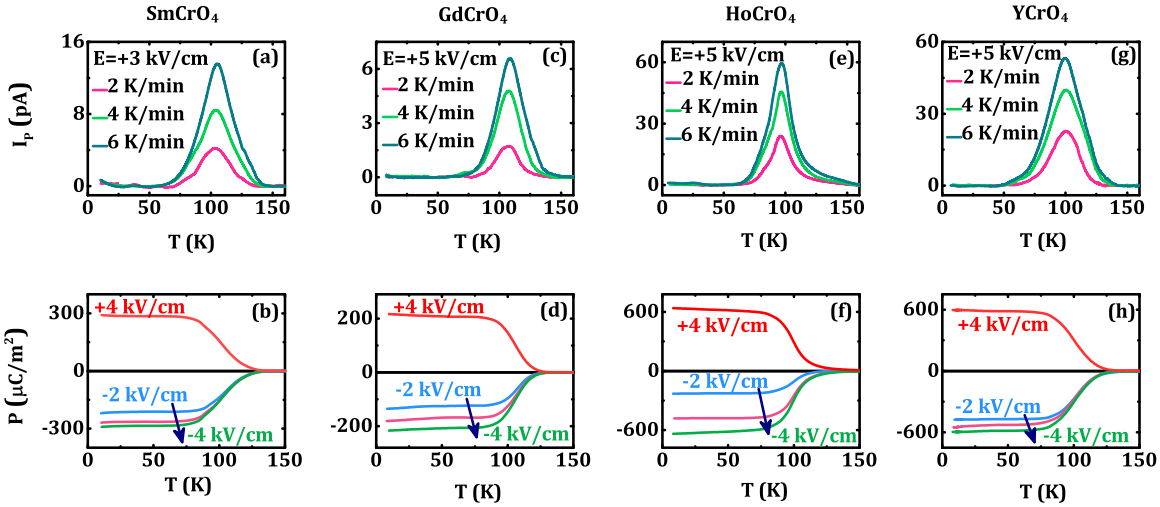

FIG. 7. The T variations of pyroelectric current (I_p) at different thermal sweep rates of (a) $SmCrO_4$ for + 3 kV/cm poling field, (c) $GdCrO_4$, (e) $HoCrO_4$, and (g) $YCrO_4$ for + 5 kV/cm poling field. The T variations of polarization (P) estimated at different poling fields for (b) $SmCrO_4$, (d) $GdCrO_4$, (f) $HoCrO_4$, and (h) $YCrO_4$.

$YCrO_4$ are depicted in Figs. 8(c) and 8(f), respectively, which display a considerable decrease in the intensity below the FE T_Cs. These signatures around FE T_C may involve changes to the scattering cross section and hence a change in the scattering amplitude may be correlated to the intensity change, pointing to a possible structural transition. The change in intensity is similar to that observed for the reported ferroelectric materials,

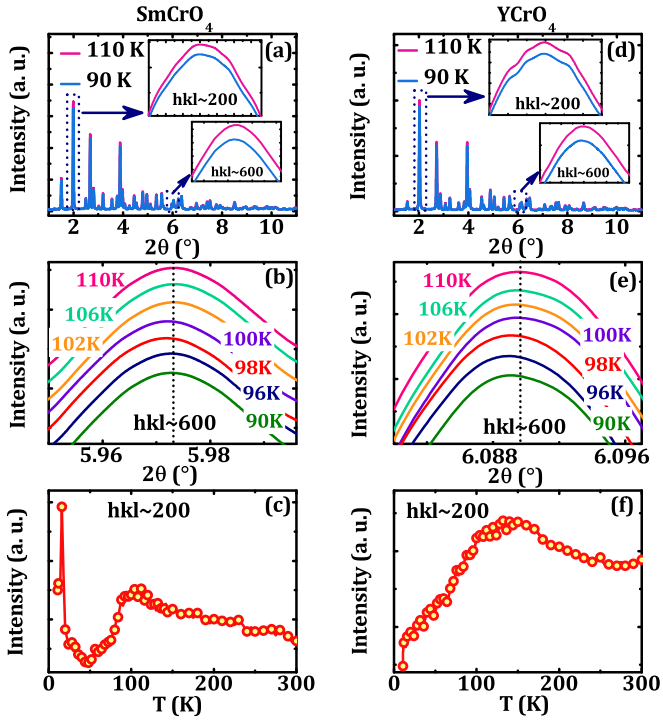

FIG. 8. Synchrotron diffraction patterns at 90 and 110 K for (a) $SmCrO_4$ and (d) $YCrO_4$. Insets highlight changes in (200) and (600) peaks. T variations of the (600) peak positions for (b) $SmCrO_4$ and (e) $YCrO_4$ and integrated intensities of (200) peak for (c) $SmCrO_4$ and (f) $YCrO_4$.

where FE T_C appeared at the structural transition temperature [44,49,54]. For $SmCrO_4$, the integrated intensity exhibits a minimum at ~50 K, around which a weak anomaly is observed in both the ZFC and FC magnetization curves, as depicted in the inset of Fig. 2(a). This points to a magnetoelastic coupling. With further decreasing temperature a sharp peak is observed around T_N, as depicted in Fig. 8(c), which is a strong signature of the magneto-elastic coupling. Possible occurrence of the magnetoelastic coupling for $YCrO_4$ ($T_N = 9$ K) is beyond the scope of our synchrotron data, which is recorded up to 10 K. Nevertheless, the intensity changes of the (200) peak for $SmCrO_4$ and $YCrO_4$ below their respective FE T_Cs indicate a signature of the structural transformation. The diffraction patterns are refined with the high-temperature $I4_1/amd$ space group in the entire recorded temperature range. We note that the refinement is not satisfactory below the FE T_C for both $SmCrO_4$ and $YCrO_4$. Moreover, the lattice parameters show a jump around the FE T_C. Thus a structural transformation from $I4_1/amd$ to a noncentrosymmetric structure is proposed for justifying the occurrence of polar order. We incorporate AMPLIMODE [55] and ISODISTORT [56] softwares to find out possible noncentrosymmetric space groups below the FE T_C. We note that the $I\bar{4}2d$ (122) space group has the highest symmetry among all possible noncentrosymmetric structures. The best fit with the $I\bar{4}2d$ space group is realized with coordinates of Sm (0, 0, 0.5), Cr (0, 0, 0), O (0.4812, 0.1826, 0.9234), and lattice constants, $a = 7.2514(5)$, $c = 6.3488(7)$ Å for $SmCrO_4$ and Y (0, 0, 0.5), Cr (0, 0, 0), O (0.5068, 0.1788, 0.9202), and the lattice constants $a = 7.1128(5)$ and $c = 6.2458(2)$ Å for $YCrO_4$. Examples of the fits at 90 K for $SmCrO_4$ and $YCrO_4$ are shown in Figs. 9(b) and 9(d), respectively, with a noncentrosymmetric $I\bar{4}2d$ space group. In order to justify the satisfactory fit, Rietveld refinements of the diffraction patterns are done for both using the high-temperature $I4_1/amd$ space group, as depicted in Figs. 9(a) and 9(c). Insets of the figures clearly demonstrate the refinements in a small 2θ range and authenticate the better fits of the diffraction patterns using $I\bar{4}2d$ than the $I4_1/amd$ space group with the small reliability

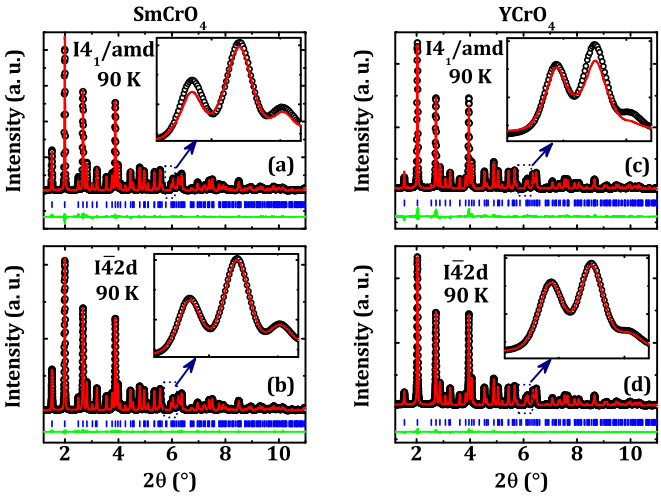

FIG. 9. Rietveld refinements of the diffraction patterns at 90 K for (a) $SmCrO_4$ and (c) $YCrO_4$ using $I4_1/amd$ space group, and for (b) $SmCrO_4$ and (d) $YCrO_4$ using $I\bar{4}2d$ space group. The inset further highlights the quality of the refinements in a small 2θ region.

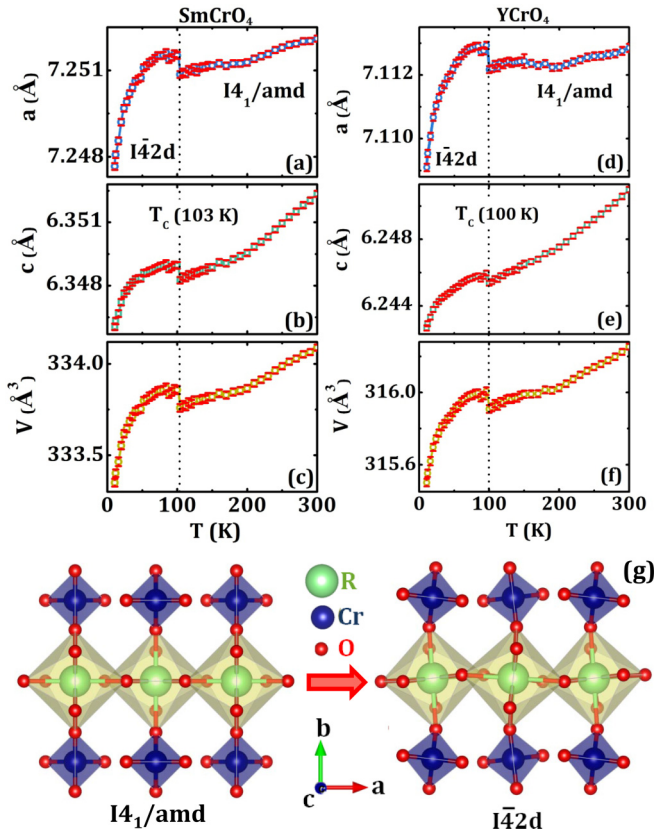

FIG. 10. The T variations of lattice parameters (a) a, (b) c, and (c) volume, V, for $SmCrO_4$, and (d) a, (e) c, and (f) V for $YCrO_4$. Vertical broken lines show the corresponding FE T_Cs. (g) Distortions of RO_8 and CrO_4 polyhedra above and below FE T_C.

parameters $R_w(\%)$ ~4.08, $R_{\exp}(\%)$ ~3.02, and $\sigma \sim 0.017$ for $SmCrO_4$ and $R_w(\%)$ ~4.29, $R_{\exp}(\%)$ ~3.29, and $\sigma \sim 0.012$ for $YCrO_4$. The bars below the diffraction patterns represent the diffraction peak positions and the difference plots are shown at the bottom for all the refinements. The difference plots shown at the bottom confirm a single phase without trace amount of impurity.

Thermal variations of the lattice parameters, a and c, as obtained from the refinements, are depicted in Figs. 10(a), 10(b) and 10(d), 10(e) for $SmCrO_4$ and $YCrO_4$, respectively. The FE T_Cs are shown by the vertical broken lines in the figures. Identical changes of $a(T)$ and $c(T)$ are observed for both the compounds. A steplike change around FE T_C is observed in $a(T)$ and $c(T)$ for both $SmCrO_4$ and $YCrO_4$, respectively. Below T_Cs, both $a(T)$ and $c(T)$ remain unchanged up to ~80 K, below which they decrease with further decreasing temperature. Similar changes in the thermal variation of unit cell volume (V) are depicted in Figs. 10(c) and 10(f) for $SmCrO_4$ and $YCrO_4$, respectively. We note that the steplike volume increases are ~0.031% and ~0.028% for $SmCrO_4$ and $YCrO_4$, respectively. The results demonstrate that the ferroelectricity in both $SmCrO_4$ and $YCrO_4$ is correlated this structural transition from the centrosymmetric $I4_1/amd$ to a noncentrosymmetric $I\bar{4}2d$ structure. In the centrosymmetric $I4_1/amd$ structure, the RO_8 dodecahedra are connected to one another through the common edges of the CrO_4 tetrahedral units, as depicted in Fig. 10(g). The considerable deformations of CrO_4 tetrahedra and RO_8 dodecahedra attributed to the structural change are also depicted in Fig. 10(g). In order to understand these deformations microscopically, the bond lengths and bond angles between different atoms are investigated further.

The Cr-O bond lengths and O-Cr-O bond angles are calculated around FE T_C for both $SmCrO_4$ and $YCrO_4$. Thermal variations of Cr-O bond length ($d_{\text{Cr–O}}$) and two O-Cr-O bond angles are shown in Figs. 11(a)–11(c) and 11(d)–11(f) for $SmCrO_4$ and $YCrO_4$, respectively. Two possible O-Cr-O bond angles, defined as α_1 and α_2, are described in the inset of Figs. 11(e) and 11(f). A steplike sharp jump is observed in $d_{\text{Cr–O}}$ at FE T_Cs for both the compounds. We note that the changes in $d_{\text{Cr–O}}$ at FE T_C are ~0.17% and ~0.24% for $SmCrO_4$ and $YCrO_4$, respectively. A decrease and increase are observed in α_1 and α_2, respectively, around the FE T_C in a similar way for both the compounds. The maximum values of changes in α_1 and α_2 below FE T_C are remarkable as ~0.07% and ~0.18%, respectively, for $SmCrO_4$, which are ~0.11% and ~0.25%, respectively, for α_1 and α_2 in case of $YCrO_4$. The microscopic parameters clearly demonstrate that these changes are considerably larger for $YCrO_4$ than $SmCrO_4$, and implies that the deformation of CrO_4 tetrahedra in $YCrO_4$ is larger than $SmCrO_4$. A schematic representation of the distortions of CrO_4 tetrahedra is illustrated in Fig. 11(g). Here, the oxygen atoms move away from the Cr atoms, which are indicated by the arrows in the middle CrO_4 tetrahedral unit, as an example. In addition, opposite rotations of consecutive tetrahedra are noted involving the structural transition at FE T_C.

We calculate the bond lengths, $d_{\text{Sm–O}}$ and $d_{\text{Y–O}}$ in the SmO_8 and YO_8 dodecahedra, respectively, around FE T_C. The thermal variations of $d_{\text{Sm–O}}$ and $d_{\text{Y–O}}$ are depicted in Figs. 12(a) and 12(c) for $SmCrO_4$ and $YCrO_4$, respectively. Opposite behavior between $d_{\text{Sm–O}}(T)$ and $d_{\text{Y–O}}(T)$ is observed. A sharp steplike rise of ~0.34% is noted for $d_{\text{Sm–O}}(T)$, in contrast to the steplike fall of ~0.11% for $d_{\text{Y–O}}(T)$. The results

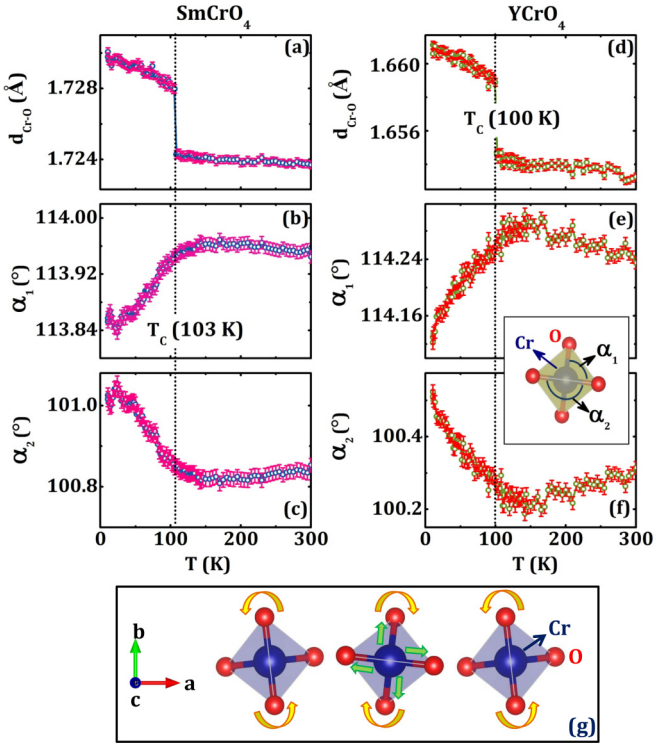

FIG. 11. The T variations of (a) $d_{Cr–O}$, bond angles (b) α_1 and (c) α_2 for $SmCrO_4$, and (d) $d_{Cr–O}$, bond angle (e) α_1 and (f) α_2 for $YCrO_4$. The insets of (e) and (f) describe α_1 and α_2. (g) Schematic diagram of distortion of the CrO_4 tetrahedra below FE T_C exhibiting rotations of CrO_4 octahedra and displacements of O atoms, as indicated by the arrows.

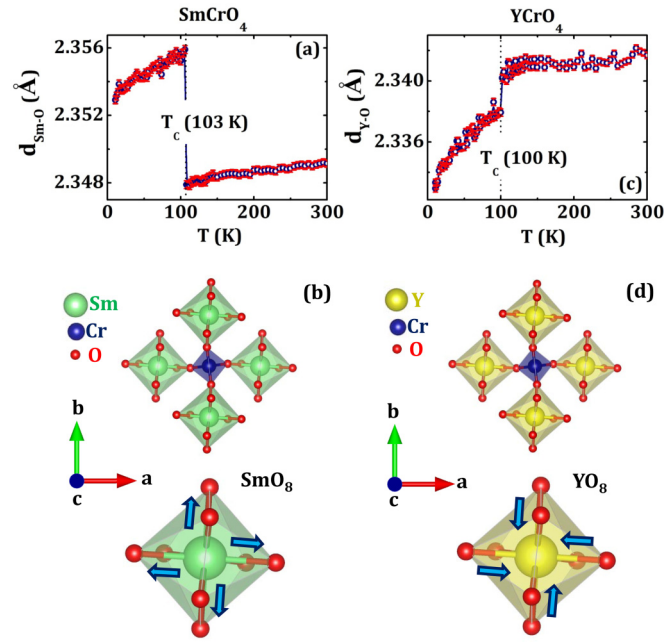

FIG. 12. The T variations of (a) $d_{Sm–O}$ for $SmCrO_4$ and (c) $d_{Y–O}$ for $YCrO_4$. Schematic diagram of connected two types of CrO_4 and $(R,Y)O_8$ polyhedra in (b) $SmCrO_4$ and (d) $YCrO_4$ displaying deformations. Expansion and contraction of $(R,Y)O_8$ polyhedra for $SmCrO_4$ and $YCrO_4$ are shown in the bottom panels of (b) and (d), respectively.

imply an expansion of SmO_8 dodecahedra in contrast to the contraction of YO_8 dodecahedra at FE T_C. In addition, the distortion of $(R,Y)O_8$ unit is less for $YCrO_4$ than the value for $SmCrO_4$. Since the CrO_4 tetrahedra and YO_8 dodecahedra are connected to each other, the contraction of YO_8 strongly influences deformation by the expansion of CrO_4 tetrahedra in order to accommodate a change in the unit cell volume around the FE order for $YCrO_4$. Thus the microstructural results infer that the polarization value of $YCrO_4$ is not so influential with the $(R,Y)O_8$ distortion, rather involved with the CrO_4 distortion. The larger CrO_4 distortion leads to the larger polarization value for $YCrO_4$ than $SmCrO_4$.

The delicate interplay between structural distortions and the observed ferroelectric properties recently attracts significant attention in the community. Structural correlations to the ferroelectric order have been investigated for the various films [57–62] as well as polycrystalline compounds [63–65]. The epitaxial strain driven enhancement of the ferroelectric properties was recently observed for the films of $TbMnO_3$ [57], $BaTiO_3$ [58], and $BiFeO_3$ [59,60]. In contrast, a possible correlation between strain and ferroelectricity for the epitaxial $BiFeO_3$ [61] and $PbZr_{0.2}Ti_{0.8}O_3$ films was not established [62]. In addition to the important results for films, the magnetoelastic couplings were found instrumental for the large polarization in bulk perovskite systems, which was addressed from first-principles calculations [63]. A structural distortion driven larger spontaneous ferroelectric polarization was proposed for the polycrystalline $ABi_2Ta_2O_9$ (A = Ca, Sr, and Ba) [64]. Recently, the crystal structural distortion was suggested as a rich playground for tuning the polarization value in case of multiferroic $Ca_{1-x}La_xBaCo_4O_7$ ($x \leqslant 0.05$) [65]. Analogous to these reported results, the higher CrO_4 distortion leads to the larger polarization value for $YCrO_4$ than $SmCrO_4$. Another significant observation is that the FE T_Cs are much higher than the magnetic ordering temperatures for all the $RCrO_4$ series. This is also analogous to that described in few members of $RCrO_3$ series, where onsets of the FE orders were observed above the magnetic ordering temperatures for R = Sm, Gd, Ho, and Lu [51,52,66,67]. The structural transition to a noncentrosymmetric structure of $Pna2_1$ from the centrosymmetric $Pbnm$ structure was found to be associated with the polar order. The rotations of CrO_6 octahedra were proposed to be correlated with the structural transition as well as emergence of the polar orders for Sm, Ho, and Gd chromates [51,52,68]. Analogous scenario is observed in the current investigation, where the rotation of CrO_4 unit is involved with the structural transition from the centrosymmetric $I4_1/amd$ structure to a noncentrosymmetric $I\bar{4}2d$ structure. Here, opposite rotations in the CrO_4 tetrahedra are noticed involving structural transition for $(R,Y)CrO_4$, similar to the CrO_6 octahedral rotations involving analogous structural transition to the noncentrosymmetric structure for interpreting occurrence of the polar order. In fact, a unique possibility of hybrid ferroelectricity was originally proposed by Benedek *et al.* involving octahedral rotations [69,70]. Current observation further proposes occurrence of the polar order involving CrO_4 tetrahedral rotations and provides the scopes for further theoretical calculations in

$(R,Y)CrO_4$ series. Here, onset of the FE order associated with the structural transition ranges from 98 to 108 K, which is well below a significant temperature, below which the inverse susceptibility deviates from the Curie-Weiss behavior for all $(R,Y)CrO_4$. The results propose that dominant short-range order driven structural change breaks the space inversion symmetry, and eventually the ferroelectric order emerges in $(R,Y)CrO_4$. Further studies in other members of this series and the theoretical calculations are suggested for establishing a possible origin of the structural change and the ferroelectric order in an unexplored $(R,Y)CrO_4$ series.

IV. CONCLUSIONS

The results of $(R,Y)CrO_4$ series propose a new family of multiferroics. The ferroelectric ordering temperature is observed at reasonably high temperatures from 98 to 108 K associated with the large values of polarization ranging from $\sim$217 to $\sim$640 $\mu C/m^2$. The large polarization value of $YCrO_4$ compared to the value of $SmCrO_4$ is attributed to the larger distortion of CrO_4 tetrahedra. The structural transition to a noncentrosymmetric $I\bar{4}2d$ space group from the centrosymmetric $I4_1/amd$ structure is found to be correlated with the occurrence of polar order.

ACKNOWLEDGMENTS

S.G. acknowledges SERB, India project (Project No. SB/S2/CMP-029/2014) for the financial support. S.G. also acknowledges DST, India for the financial support to perform experiment at PETRA III, DESY, Germany for synchrotron diffraction studies (Proposal No. I-20150193).

[1] A. A. Tsirlin, M. G. Rabie, A. Efimenko, Z. Hu, R. Saez-Puche, and L. H. Tjeng, Phys. Rev. B **90**, 085106 (2014).
[2] A. Ray and T. Maitra, J. Phys.: Condens. Matter **27**, 105501 (2015).
[3] A. P. Dickin, *Radiogenic Isotope Geology* (Cambridge University Press, New York, 1995), p. 490.
[4] *Reviews in Mineralogy*, edited by J. M. Hanchar and P. W. O. Hoskin (Mineralogical Society of America, Washington, D.C., 2003), Vol. 53.
[5] V. S. Stubican and R. Roy, Z. Kristallogr. **119**, 90 (1963).
[6] Y. W. Long, L. X. Yang, Y. Yu, F. Y. Li, R. C. Yu, S. Ding, Y. L. Liu, and C. Q. Jin, Phys. Rev. B **74**, 054110 (2006).
[7] X. Wang, I. Loa, K. Syassen, M. Hanfland, and B. Ferrand, Phys. Rev. B **70**, 064109 (2004).
[8] Y. W. Long, L. X. Yang, Y. Yu, F. Y. Li, R. C. Yu, and C. Q. Jin, Phys. Rev. B **75**, 104402 (2007).
[9] J. Sivardiere, Phys. Rev. B **8**, 2004 (1973).
[10] A. H. Cooke, D. M. Martin, and M. R. Wells, Solid State Commun. **9**, 519 (1971).
[11] J. C. Wright and H. W. Moos, Phys. Rev. B **4**, 163 (1971).
[12] C. J. Jia, L. D. Sun, F. Luo, X. C. Jiang, L. H. Wei, and C. H. Yan, Appl. Phys. Lett. **84**, 5305 (2004).
[13] J. K. Jabczynski, W. Zendzian, and J. Kwiatkowski, Opt. Express **14**, 2184 (2006).
[14] H. Bischoff, B. Pilawa, A. Kasten, and H. G. Kahle, J. Phys.: Condens. Matter **3**, 10057 (1991).
[15] P. Radhakrishna, J. Hammann, and P. Pari, J. Magn. Magn. Mater. **23**, 254 (1981).
[16] V. A. Gubanov, R. N. Pletnev, V. N. Lisson, and A. K. Chirkov, Spectrosc. Lett. **10**, 527 (1977).
[17] A. H. Cooke, C. J. Ellis, K. A. Gehring, M. J. M. Leask, D. M. Martin, B. M. Wanklyn, M. R. Wells, and R. L. White, Solid State Commun. **8**, 689 (1970).
[18] B. Daudin, Solid State Commun. **48**, 639 (1970).
[19] A. A. Demidov and N. P. Kolmakova, Physica B **363**, 245 (2005).
[20] M. Moussa, M. Djermouni, S. Kacimi, M. Azzouz, A. Dahani, and A. Zaoui, Comput. Mater. Sci. **68**, 361 (2013).
[21] K. Dey, A. Indra, S. Majumdar, and S. Giri, J. Mater. Chem. C **5**, 1646 (2017).
[22] E. Jiménez, J. Isasi, and R. Sáez-Puche, J. Solid State Chem. **164**, 313 (2002).
[23] E. Jiménez, J. Isasi, and R. Sáez-Puche, J. Alloys Compd. **312**, 53 (2000).
[24] K. Tezuka and Y. Hinatsu, J. Solid State Chem. **160**, 362 (2001).
[25] A. Morales-Sánchez, F. Fernández, and R. Sáez-Puche, J. Alloys Compd. **201**, 161 (1993).
[26] E. Jimenez, P. Bonville, J. A. Hodges, P. C. M. Gubbens, J. Isasi, and R. Saez-Puche, J. Magn. Magn. Mater. **272–276**, 571 (2004).
[27] Y. W. Long, Q. Huang, L. X. Yang, Y. Yua, Y. X. Lv, J. W. Lynn, Y. Chen, and C. Q. Jin, J. Magn. Magn. Mater. **322**, 1912 (2010).
[28] E. Jiménez-Melero, P. C. M. Gubbens, M. P. Steenvoorden, S. Sakarya, A. Goosens, P. Dalmas de Réotier, A. Yaouanc, J. Rodríguez-Carvajal, B. Beuneu, J. Isasi, R. Sáez-Puche, U. Zimmerman, and J. L. Martínez, J. Phys.: Condens. Matter **18**, 7893 (2006).
[29] R. Sáez-Puche, E. Jiménez, J. Isasi, M. T. Fernández-Díaz, and J. L. García-Muñoz, J. Solid State Chem. **171**, 161 (2003).
[30] M. Steiner and H. Dachs, Solid State Commun. **29**, 231 (1979).
[31] R. Sáez Puche, E. Climent, M. G. Rabie, J. Romero, and J. M. Gallardo, J. Phys.: Conf. Ser. **325**, 012012 (2011).
[32] A. J. Dos santos-García, E. Climent-Pascual, J. M. Gallardo-Amores, M. G. Rabie, Y. Doi, J. Romero de Paz, B. Beuneu, and R. Saéz-Puche, J. Solid State Chem. **194**, 119 (2012).
[33] E. Jimenez-Melero, N. H. van Dijk, W. H. Kraan, P. C. M. Gubbens, J. Isasi, and R. Saez-Puche, J. Magn. Magn. Mater. **288**, 1 (2005).
[34] E. Jiménez, W. H. Kraan, N. H. van Dijk, P. C. M. Gubbens, J. Isasi, and R. Sáez-Puche, Physica B **350**, e293 (2004).
[35] Y. Long, Q. Liu, Y. Lv, R. Yu, and C. Jin, Phys. Rev. B **83**, 024416 (2011).
[36] E. Palacios, C. Tomasi, R. Sáez-Puche, A. J. Dos santos-García, F. Fernández-Martínez, and R. Burriel, Phys. Rev. B **93**, 064420 (2016).
[37] A. Midya, N. Khan, D. Bhoi, and P. Mandal, Appl. Phys. Lett. **103**, 092402 (2013).
[38] A. Midya, N. Khan, D. Bhoi, and P. Mandal, J. Appl. Phys. **115**, 17E114 (2014).
[39] E. Climent, J. M. Gallardo, J. Romero de Paz, N. Tairaa, and R. Sáez Puche, J. Alloys Compd. **488**, 524 (2009).
[40] E. Climent-Pascual, J. Romero de Paz, J. Manuel Gallardo-Amores, and R. Saéz-Puche, Solid State Sci. **9**, 574 (2007).

[41] Y. Aoki, H. Konno, and H. Tachikawa, J. Mater. Chem. **11**, 1214 (2001).
[42] D. Errandonea, R. Kumar, J. López-Solano, P. Rodríguez-Hernández, A. Muñoz, M. G. Rabie, and R. Sáez Puche, Phys. Rev. B **83**, 134109 (2011).
[43] A. Ray and T. Maitra, AIP Conf. Proc. **1832**, 090017 (2017).
[44] K. Dey, A. Karmakar, A. Indra, S. Majumdar, U. Rutt, O. Gutowski, M. v. Zimmermann, and S. Giri, Phys. Rev. B **92**, 024401 (2015).
[45] T. D. Sparks, M. C. Kemei, P. T. Barton, R. Seshadri, E.-D. Mun, and V. S. Zapf, Phys. Rev. B **89**, 024405 (2014).
[46] N. Mufti, A. A. Nugroho, G. R. Blake, and T. T. M. Palstra, J. Phys.: Condens. Matter **22**, 075902 (2010).
[47] T. Kimura, S. Kawamoto, I. Yamada, M. Azuma, M. Takano, and Y. Tokura, Phys. Rev. B **67**, 180401(R) (2003).
[48] J. K. Dey, S. Majumdar, and S. Giri, J. Phys.: Condens. Matter **30**, 235801 (2018).
[49] A. Indra, K. Dey, S. Majumdar, I. Sarkar, S. Francoual, R. P. Giri, N. Khan, P. Mandal, and S. Giri, Phys. Rev. B **95**, 094402 (2017).
[50] N. Terada, Y. S. Glazkova, and A. A. Belik, Phys. Rev. B **93**, 155127 (2016).
[51] A. Ghosh, K. Dey, M. Chakraborty, S. Majumdar, and S. Giri, Europhys. Lett. **107**, 47012 (2014).
[52] A. Ghosh, A. Pal, K. Dey, S. Majumdar, and S. Giri, J. Mater. Chem. C **3**, 4162 (2015).
[53] K. Dey, A. Indra, D. De, S. Majumdar, and S. Giri, ACS Appl. Mater. Interfaces **8**, 12901 (2016).
[54] K. Dey, S. Majumdar, and S. Giri, Phys. Rev. B **90**, 184424 (2014).
[55] D. Orobengoa, C. Capillas, I. Aroyo, and J. M. Perez-Mato, J. Appl. Crystallogr. **42**, 820 (2009).
[56] B. J. Campbell, H. T. Stokes, D. E. Tanner, and D. M. Hatch, J. Appl. Crystallogr. **39**, 607 (2006).
[57] K. Shimamoto, S. Mukherjee, S. Manz, J. S. White, M. Trassin, M. Kenzelmann, L. Chapon, T. Lippert, M. Fiebig, C. W. Schneider, and C. Niedermayer, Sci. Rep. **7**, 44753 (2017).
[58] C. Dubourdieu, J. Bruley, T. M. Arruda, A. Posadas, J. Jordan-Sweet, M. M. Frank, E. Cartier, D. J. Frank, S. V. Kalinin, A. A. Demkov, and V. Narayanan, Nat. Nanotech. **8**, 748 (2013).
[59] H.-J. Liu, C.-W. Liang, W.-I. Liang, H.-J. Chen, J.-C. Yang, C.-Y. Peng, G.-F. Wang, F.-N. Chu, Y.-C. Chen, H.-Y. Lee, L. Chang, S.-J. Lin, and Y.-H. Chu, Phys. Rev. B **85**, 014104 (2012).
[60] C. Daumont, W. Ren, I. C. Infante, S. Lisenkov, J. Allibe, C. Carrétéro, S. Fusil, E. Jacquet, T. Bouvet, F. Bouamrane, S. Prosandeev, G. Geneste, B. Dkhil, L. Bellaiche, A. Barthélémy, and M. Bibes, J. Phys.: Condens. Mater **24**, 162202 (2012).
[61] D. H. Kim, H. N. Lee, M. D. Biegalski, and H. M. Christen, Appl. Phys. Lett. **92**, 012911 (2008).
[62] H. N. Lee, S. M. Nakhmanson, M. F. Chisholm, H. M. Christen, K. M. Rabe, and D. Vanderbilt, Phys. Rev. Lett. **98**, 217602 (2007).
[63] H. J. Zhao, L. Bellaiche, X. M. Chen, and J. Íñiguez, Nat. Commun. **8**, 14025 (2017).
[64] Y. Shimakawa, Y. Kubo, Y. Nakagawa, S. Goto, T. Kamiyama, H. Asano, and F. Izumi, Phys. Rev. B **61**, 6559 (2000).
[65] K. Dey, A. Indra, A. Chatterjee, S. Majumdar, U. Rütt, O. Gutowski, M. v. Zimmermann, and S. Giri, Phys. Rev. B **96**, 184428 (2017).
[66] K. R. S. Preethi Meher, C. Martin, V. Caignaert, F. Damay, and A. Maignan, Chem. Mater. **26**, 830 (2014).
[67] K. R. S. Preethi Meher, A. Wahl, A. Maignan, C. Martin, and O. I. Lebedev, Phys. Rev. B **89**, 144401 (2014).
[68] S. Mahana, B. Rakshit, R. Basu, S. Dhara, B. Joseph, U. Manju, S. D. Mahanti, and D. Topwal, Phys. Rev. B **96**, 104106 (2017).
[69] N. A. Benedek, A. T. Mulder, and C. J. Fennie, J. Solid State Chem. **195**, 11 (2012).
[70] N. A. Benedek and C. J. Fennie, Phys. Rev. Lett. **106**, 107204 (2011).